Multiscale analysis of waves reflected by granular media: Acoustic experiments on glass beads and effective medium theories

Yves Le Gonidec, Dominique Gibert

Multiscale analysis of waves reflected by granular media: Acoustic experiments on glass beads and effective medium theories

Yves Le Gonidec[1,2] and Dominique Gibert[1,3]

Received 19 May 2006; revised 20 November 2006; accepted 13 December 2006; published 10 May 2007.

[1] The wavelet response is a multiscale method based on the continuous wavelet transform. We use it to characterize the acoustic reflectivity of a layer of glass beads with diameter $d = 1$ mm randomly arranged in water. The volumetric concentration is $\phi \simeq 63\%$ of spherical inclusions. The wavelet response is measured over a large frequency range (100 kHz $\leq f \leq$ 5 MHz) where five different acoustic regimes are identified on the basis of scattering phenomena. A strong decrease in the reflectivity occurs when the wavelength of the incident wave is twice the bead diameter, a situation where lateral scattering is dominant. The energy ratio of the ballistic and the coda parts of the wavelet response reveals a clear transition from a ballistic propagation regime to a diffusion regime where multiple scattering occurs. The experimental data are explained with an effective medium theory approach: the reflectivity data in the low-frequency domain of the spanned frequency range are correctly reproduced with quasi-static models. For higher frequencies, more sophisticated models accounting for multiple scattering must be used. The high-frequency part of the experimental reflectivity curve may be explained by strong multiple scattering at the top of the glass beads located at the surface of the layer and corresponds to the optical geometric limit.

Citation: Le Gonidec, Y., and D. Gibert (2007), Multiscale analysis of waves reflected by granular media: Acoustic experiments on glass beads and effective medium theories, *J. Geophys. Res.*, *112*, B05103, doi:10.1029/2006JB004518.

1. Introduction

[2] The nondestructive characterization of heterogeneous geological materials with either seismic or electromagnetic waves is an important issue which has motivated numerous studies concerned with the heterogeneous properties of the Earth from the global scale [*Wysession et al.*, 1992; *Chambers et al.*, 2005] down to the very small scales encountered in environmental and engineering applications [*Exon et al.*, 1998; *Pecher et al.*, 2003]. Near-surface layers also constitute an increasing matter of interest for either pollution concerns or safety assessment of civil engineering equipments. An example pertaining to the civil engineering industry concerns the characterization of the sea bottom [*Schock et al.*, 1989; *De Moustier and Matsumoto*, 1993; *Augustin et al.*, 1996; *Orange et al.*, 2002; *Acosta et al.*, 2004] for the purpose of planning the installation of optic fiber networks and communication cables or to identify resources for future mining and fishing facilities [*Carter*, 1992; *McClatchie et al.*, 2000; *Kostylev et al.*, 2001].

[3] Acoustic probing of heterogeneous interfaces requires a good knowledge of wave propagation inside the structures where strong interactions between the acoustic wave and the medium heterogeneities can occur. The interpretation of these phenomena is not straightforward: geological reflectors are complex, multiphase interfaces (i.e., mixtures of fluids, rocks and gas). For instance, the seafloor consists of different sedimental components (e.g., mud, silt, sand, lava) mixed with water, constituting heterogeneous substrates [*Goff et al.*, 2000; *Le Gonidec et al.*, 2005]. The main physical parameters derived from echo sounder data are the velocity and the attenuation of the coherent waves, i.e., the specular reflections. Attenuation of broadband Chirp signals is used for sediment classification [*Vandenplas et al.*, 2000; *Stevenson et al.*, 2002; *Gutowski et al.*, 2002]. Attenuation is frequency-dependent, and new acoustic techniques use multifrequency methods [*Vanneste et al.*, 2001; *Walter et al.*, 2002; *Lambert et al.*, 2002; *Price*, 2006].

[4] Wave propagation inside complex media has been intensively described and has motivated numerous studies [e.g., *O'Doherty and Anstey*, 1971; *Sheng et al.*, 1986; *Burridge et al.*, 1988, 1993; *Scales*, 1993; *Page et al.*, 1995; *Cowan et al.*, 1998; *Derode et al.*, 1998; *Tournat et al.*, 2004; *Marchetti et al.*, 2004; *Dineva et al.*, 2006]. The interaction of the acoustic wave with a complex interface is strongly controlled by the ratio λ/d of the incident wavelength to the heterogeneity size [*Le Gonidec et al.*, 2002]: At the macroscopic scale, when the wavelength λ is much

[1] Géosciences Rennes, CNRS/INSU UMR 6118, Université Rennes 1, Rennes, France.
[2] Now at Géosciences Azur, CNRS/INSU UMR 6526, Observatoire Océanologique de Villefranche-sur-Mer, Villefranche-sur-Mer, France.
[3] Also at GdR Formations Géologiques Profondes, CNRS/Agence Nationale pour la gestion des Déchets Radioactifs, Rennes, France.

0148-0227/07/2006JB004518$09.00

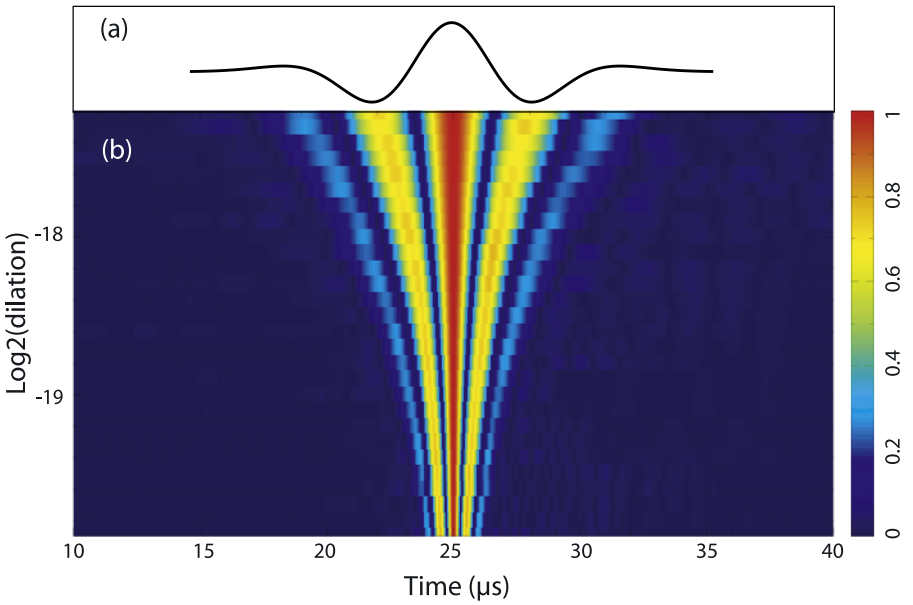

Figure 1. (a) One member of the experimental wavelet family. Each wavelet is inverted in order to best fit with the fourth derivative of a Gaussian: $(d^4/dt^4)\exp(-t^2)$. (b) Assemblage of the whole experimental wavelet family obtained by ranking each wavelet with respect to its dilation inversely proportional to its central frequency.

larger than the microstructure characteristic size d, the Rayleigh regime dominates and static effective medium theories provide a useful framework to derive the macroscopic properties of composite materials [e.g., *Chýlek et al.*, 2000]. Such static methods describe the frequency-independent properties of the equivalent homogeneous medium and has been studied by many authors [*Foldy*, 1945; *Hashin and Shtrikman*, 1963; *Kuster and Toksöz*, 1974; *Berryman*, 1980; *Berryman and Berge*, 1996; *Aristégui and Angel*, 2002]. In the mesoscale domain where $\lambda \simeq d$, the interaction between the acoustic wave and the microstructure of the medium strongly depends on the ratio λ/d, and dynamic effective medium theories have been proposed to account for both the frequency-dependent properties of multiphase composites and multiple scattering [*Waterman and Truell*, 1961; *Sheng*, 1995; *Busch and Soukoulis*, 1996].

[5] In the present paper, we study the frequency dependence of the acoustic reflectivity of a layer made of a densely packed granular medium. In particular, we examine the influence of the ratio λ/d by means of the "wavelet response" introduced in a previous paper [*Le Gonidec et al.*, 2002]. Similar to the continuous wavelet transform, defined as the convolution between the analyzed signal and a family of wavelets obtained from a given analyzing function (see *Holschneider* [1995] for an introduction), the wavelet response also uses a family of wavelets which are propagated (NOT convolved) through the medium to be analyzed. The properties of the wavelet transform concerning the characterization of abrupt changes in signals [e.g., *Mallat and Hwang*, 1992; *Herrmann*, 1994; *Alexandrescu et al.*, 1995, 1996] are retrieved in the wavelet response. This method may therefore be used to remotely probe the multiscale structure of complex interfaces [*Herrmann and Staal*, 1996; *Wapenaar*, 1998, 1999; *Marsan and Bean*, 1999] and more generally of heterogeneous structures. When compared to other analyzing methods, the wavelet response characterizes the multiscale interface structure over a very large dilation range both in the time and frequency domains.

[6] In section 1, we recall the main steps of the wavelet response method and we present the acoustic experiments. We measure the wavelet response of a biphase composite medium made of a dense packing of glass beads surrounded by fluid. We analyze the acoustic response of the granular medium from the wavelet response data, and we identify five characteristic frequency ranges. In section 2, we discuss the observed macroscopic effects from a microscale point of view. We show that the scattering diagram of a single glass bead can explain the acoustic response of the granular medium. We put in evidence the propagation-to-diffusion transition. Sections 3 and 4, we introduce and compare effective medium theories with the experimental data. We define the frequency ranges where the theories agree with the data and discuss the results.

2. Acoustic Reflectivity of a Layer of Glass Beads

2.1. Principles of the Method and Experiments

[7] In order to analyze the acoustic response of a granular medium, we use the wavelet response method, a multiscale analysis technique based on the continuous wavelet transform introduced in details in previous papers [*Le Gonidec et al.*, 2002, 2003]. The main idea at the basis of the wavelet response is to use a family of incident waves whose source signals constitute a wavelet family as shown in Figure 1 (i.e., a set of signals with constant shape and different durations). The experimental wavelet family is obtained by simulated annealing [*Conil et al.*, 2004]. The advantage of this method is to span a wide frequency range while keeping a good temporal localization of the source signals, this allows an optimal identification of the signals reflected

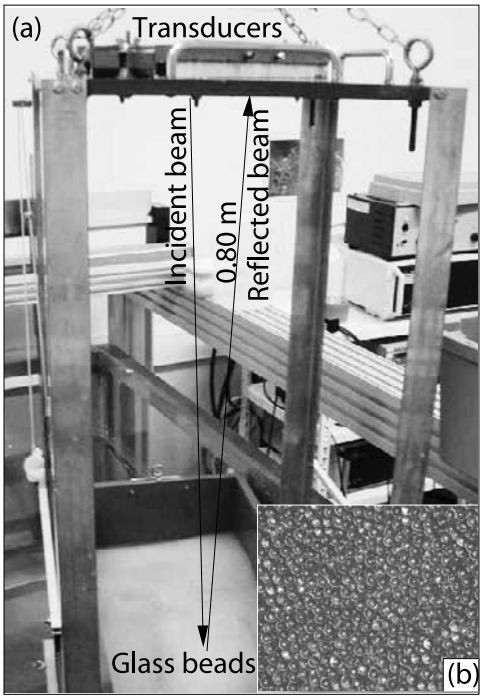

Figure 2. (a) Experimental setup holding two piezoelectric transducers above a rolling box filled with glass beads. The box can be horizontally translated while stacking the reflected signals in order to record the mean field. (b) Monodisperse glass beads randomly distributed in water. The concentration $\phi \simeq 0.63$ roughly corresponds to 10^9 beads/m^3 for $d = 1$ mm.

by the target, both in time and frequency domains. Another advantage is to avoid postprocessing operations like noise-sensitive deconvolution as often required in more conventional methods where the source signals are not controlled. The wavelet response has the further advantage to determine the homogeneity degree of a target geometry in terms of discontinuities. This has been described in previous papers [*Le Gonidec et al.*, 2002, 2003] where planar interfaces can be assimilated to Dirac-like and Heaviside-like discontinuities at low and high frequencies, respectively. A detailed account of the properties of the wavelet transform with respect to homogeneous functions is given by *Mallat and Hwang* [1992] and by *Alexandrescu et al.* [1995, 1996] for geophysical applications.

[8] The wavelet family used in the present study consists in 30 wavelets (Figure 1b) spanning a frequency range going from 200 kHz to 1 MHz. It has been generated by means of four pairs of transducers with central frequencies of 250, 500, 750, and 1000 kHz. The analyzing wavelet is the fourth derivative of a Gaussian function (Figure 1a) in order to have a well-defined central frequency while being sufficiently localized in time.

[9] The experimental setup shown in Figure 2 has already been discussed in details by *Le Gonidec et al.* [2002]. It consists in a rigid frame holding two transducers mounted in the normal incidence configuration, one for the emission and one for the reception. The acoustic reflector is a granular medium composed of a thick layer of glass beads. Both the transducers and the medium are immersed in the water of an acoustic tank. The medium is roughly 60 cm below the transducers and can be translated in order to measure the mean acoustic field in the far-field conditions. The experimental wavelet response of the medium is constructed by successively emitting each source signal (i.e., wavelet) and averaging the reflected signals.

[10] The glass beads of the granular medium are densely packed in a box, and the porosity derived from mass measurements is 37%. The concentration of the glass beads is $\phi \simeq 63\%$, typical of a random close packing [*Page et al.*, 1995, 1996] and significantly smaller than the densest concentration of 74% corresponding to a face-centered cubic packing of spherical inclusions [*Neser et al.*, 1997].

[11] A relevant nondimensional control parameter of the experiment is the ratio λ/d between the incident wavelet wavelength λ to the bead diameter d. Indeed, the granular media used in the present study have a porosity independent of the bead diameter and experimentally measured around 37% for all glass bead diameters. Then, the acoustic response of a granular medium only depends on the ratio λ/d: the glass beads are monodisperse and uniformly packed, so the wavelet responses measured for different bead diameters d may be rescaled to a common diameter and merged to obtain a global wavelet response spanning a wider range of the λ/d ratio. The wavelet response is measured for six different granular media with bead of diameters $d = 0.6$, 1, 2, 3, 4, and 5 mm, respectively. These individual wavelet responses are further rescaled at an equivalent unique diameter $d = 1$ mm and for a corresponding frequency range 100 kHz $\leq f \leq$ 5 MHz (Figure 3). We emphasize that the reference wavelet response is associated to a perfect half-space reflector.

2.2. Identification of the Coherent Frequency Bands

[12] Thanks to the controlled shape of the source signals used in the wavelet response method, the distortions observed in the wavelet response of the granular media when compared with the reference wavelet response of a perfect reflector (Figures 3a and 1b, respectively) may safely be attributed to wave phenomena produced by the heterogeneous nature of the glass bead layer. Both wavelet responses have a similar appearance at low frequency, and discrepancies are larger and larger when the frequency increases. The intermediate wavelength domain $\lambda \simeq \pi d$ marks a clear limit between the low-frequency domain where both wavelet responses look very similar with a common conical-like structure, and a high-frequency domain where the conical structure of the wavelet response becomes very complex in the case of glass beads.

[13] A quantitative analysis of the wavelet response may be done from its so-called ridge functions as detailed by *Le Gonidec et al.* [2002, 2003]. The analyzing wavelet used in the present study counts five extrema (Figure 1a) from which five ridge functions may be defined. Each ridge function is locked on a given extrema and may be followed across the dilation range spanned by the whole wavelet family. The average amplitude of the wavelet response along a given ridge function may be plotted in a log-log diagram as a function of the λ/d ratio as shown in Figure 3b. This average curve represents the reflectivity

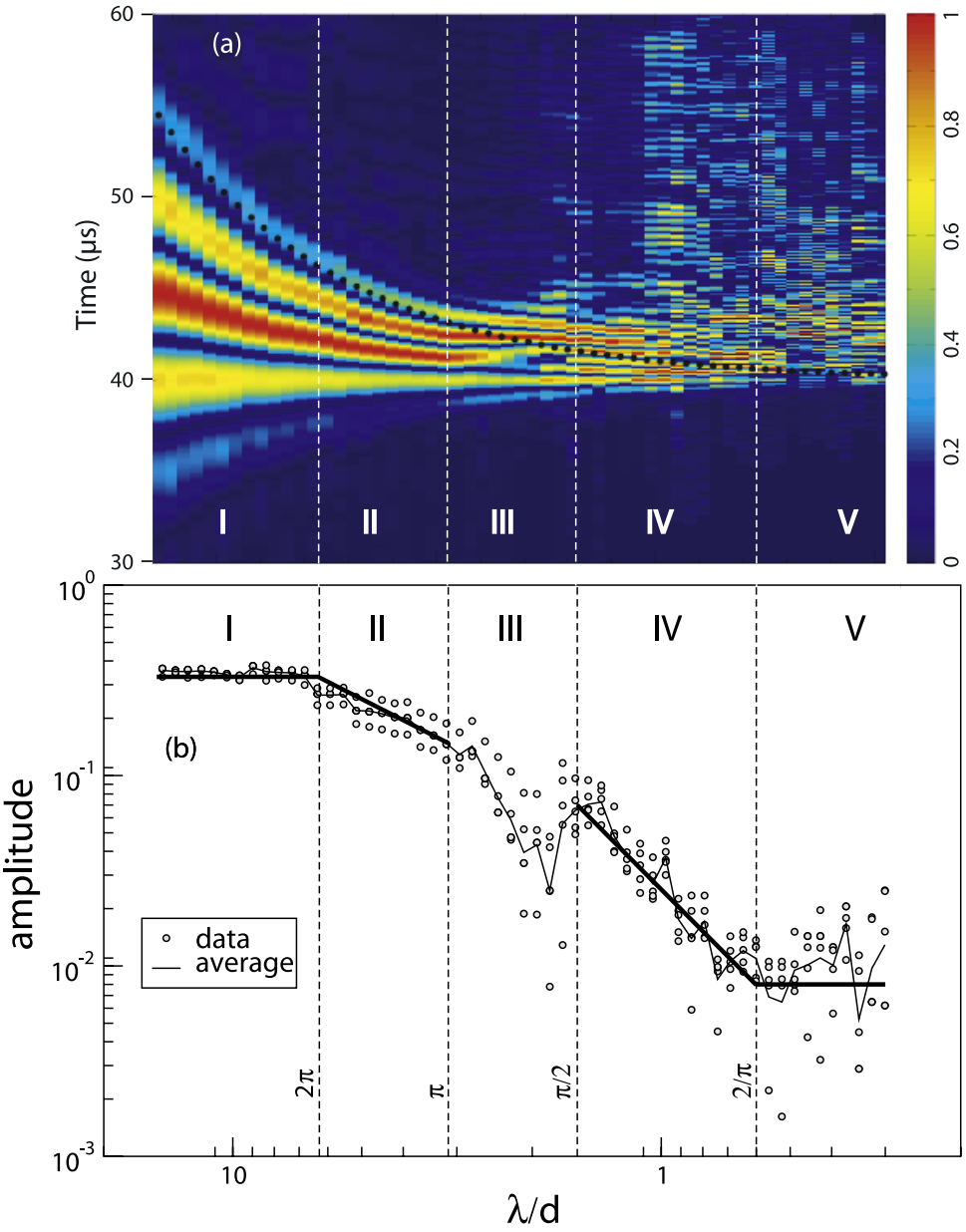

Figure 3. (a) Experimental wavelet response of a layer of glass beads with diameter d. The horizontal axis represents the nondimensional control parameter λ/d, the time axis is vertical, and the color scale represents the amplitude of the averaged reflected signal. The black dots mark the time limit of the reference wavelet shown in Figure 1: The coherent ballistic component of the wavelet response is located before this limit, and the coda component comes after. (b) Amplitude of the ballistic component of the wavelet response shown in Figure 3a. In this log-log diagram, the average curve (solid line) appears mostly linear in 4 frequency bands represented by straight segments with slopes equal to 0, +1, +2, and 0 from left to right, respectively.

curve of the layer of monodisperse glass beads, and constitutes the data which we now discuss in details.

[14] A first interpretation of the wavelet response may be done in the framework of homogeneous discontinuity analysis [*Le Gonidec et al.*, 2002, 2003]. From this point of view, the reflectivity curve may be decomposed in straight line segments with different slopes α (Figure 3b) which depend on the homogeneity degree of the discontinuity present at the acoustical interface (i.e., zero for a step-like transition). By this way, five frequency domains labeled from I to V are recognized in the experimental reflectivity curve. The limits of these domains correspond to remarkable reduced wavelengths, λ/d, represented as vertical dashed segments in Figure 3b: the corner wavelengths correspond to $\lambda = 2\pi d$, πd, $\pi d/2$ and $2\ d/\pi$, respectively.

[15] The dotted curve in Figure 3a marks the upper time limit of the wavelets used as source signals (Figure 1b). In bands I and II, the duration of the wavelet response coincides with this limit, while it is much larger in bands III, IV, and V because of the presence of a long coda wave.

2.2.1. Long-Wavelength Domain

[16] The long-wavelength domains I–II correspond to reduced wavelengths $\lambda > \pi d$ where the wavelet response of the granular medium has a simple conical appearance identical to the reference wavelet response with 5 ridge functions (Figures 3a and 1b, respectively). In these domains, the wave reflected by the surface of the granular medium appears as a single wave packet, identical to what happens for an Heaviside-like discontinuity. The distinction between domains I and II is motivated by the slope break observed in the ridge functions at $\lambda = 2d\pi$.

[17] In domain I, the ridge function is flat with $\alpha = 0$ indicating that the reflectivity does not depend on the frequency of the incident wave. The experimental reflection coefficient $R = 0.34$ is identical to the one predicted for an homogeneous half-space interface as shown in section 5.1 [*Le Gonidec et al.*, 2002].

[18] The reflectivity observed in domain II is frequency-dependent indicating that the granular medium can be assimilated to a homogeneous half-space with frequency-dependent properties. The reflectivity linearly decreases from $R = 0.34$ to $R = 0.15$ as the wavelength shortens (in a log-log plot). The frequency attenuation for glass beads $d = 1$ mm is then estimated to 0.02 dB/kHz. In section 3, we give physical interpretation of this decrease due to scattering processes which get stronger as the reduced wavelengths λ/d shortens.

2.2.2. Intermediate-Wavelength Domain

[19] Domain III covers the range $\pi d > \lambda > \pi d/2$ where the simple cone-like appearance of the wavelet response progressively disappears and splits into subconical structures at $\lambda \simeq 2d$ (Figure 3a). Observed from Figure 3b, the amplitude of the ridge functions does not obey a power law and the reflectivity curve presents a deep minimum $R \simeq 0.025$ at $\lambda \simeq 2d$. The temporal limit plotted in black dots in Figure 3a does not coincide with the time of the reference wavelet response: we observe reflected wave trains longer in time than the reference wavelets. Strong interactions occur inside the granular medium between the acoustic wave and the glass beads. We associate domain III to the transition region where the glass bead layer cannot be assimilated to a Heaviside-like interface but appears to be a complex structure.

2.2.3. Short-Wavelength Domain

[20] Domains IV–V correspond to the wavelength range $\lambda < \pi d/2$ where the reflected wave trains have a total duration much longer than the one of the reference wavelets. The reflected waves are mainly composed of a late coda typical of strong multiple scattering between the source signals and the small-scale structures of the granular medium. A strong decrease of the ridge functions is observed in domain IV with a slope $\alpha = +2$ for $\pi d/2 > \lambda > 2\, d/\pi$ where the frequency attenuation is 0.04 dB/kHz for glass beads $d = 1$ mm. In domain V, the slope of the ridge function is roughly $\alpha \simeq 0$ when $r < 2/\pi$ where the experimental data are scattered around a mean reflectivity $R \simeq 0.01$.

3. Acoustic Wave Phenomena

3.1. Definition of Scattering Parameters

[21] The amplitude f of an acoustic plane wave scattered by an inclusion depends both on the λ/d ratio and on the observation angles (θ, ϕ). For a spherical scatterer, $f(\theta, \phi) = f(\theta)$ and, in the forward scattering $\theta = 0$ and back-scattering $\theta = \pi$ directions, the far-field amplitudes are [*McClements and Povey*, 1989]

$$f(0) = \frac{1}{ik_m} \sum_{n=0}^{\infty} (2n+1) A_n \tag{1}$$

$$f(\pi) = \frac{1}{ik_m} \sum_{n=0}^{\infty} (-i)^n (2n+1) A_n, \tag{2}$$

where k is the wave number in the fluid matrix. The terms A_n [*Goodman and Stern*, 1962] include the physical properties of the materials.

[22] The scattering cross section $\sigma_s(\theta)$ is defined by

$$\sigma_s = |f(\theta)|^2 \tag{3}$$

and represents the distribution of the intensity scattered in a given direction. The total scattering cross section σ_t is defined by

$$\sigma_t = \int \sigma_s d(\theta), \tag{4}$$

and the extinction coefficient of an isolated scatterer is the total scattering cross section σ_t normalized by the geometrical cross section. For a spherical scatterer, the geometrical cross section is $\sigma_g = \pi\, d^2/4$.

[23] In average, an acoustic wave propagating in a complex medium is characterized by an exponential decay and the wave coherence disappears as the wave propagates. The corresponding distance, coherently traveled by the waves inside the heterogeneous medium until 1/3 of the incident energy is annihilated by multiple scattering, is defined as the mean free path $l(r)$:

$$l(r) = 1/n\sigma_t, \tag{5}$$

where n is the number of scatterers per volume unit and σ_t is the total scattering cross section of a single scatterer.

3.2. Small-Scale Scattering

[24] In this section, we discuss the characteristics of the scattered wavefield with respect to the five frequency bands identified from the ridge functions (Figure 3b). The results are presented as two-dimensional (2-D) radiation diagrams which are computed for a spherical scatterer with the physical properties of the glass. Figure 4a shows these diagrams representing the amplitude, $|f(\theta)|^2$, of the wavefield re-radiated by a scatterer in response to an incident wave traveling in the $\theta = \pi$ direction. The $\theta = 0$ and $\theta = \pi$ directions correspond to the longitudinal back and forward scattering directions, respectively. Transverse scattering corresponds to $\theta = \pm\pi/2$. A first glance at Figure 4a reveals that each frequency band corresponds to a particular scattering regime, from back scattering in domains I–II to forward scattering in domains IV–V. This is quantitatively assessed by examining the curves shown

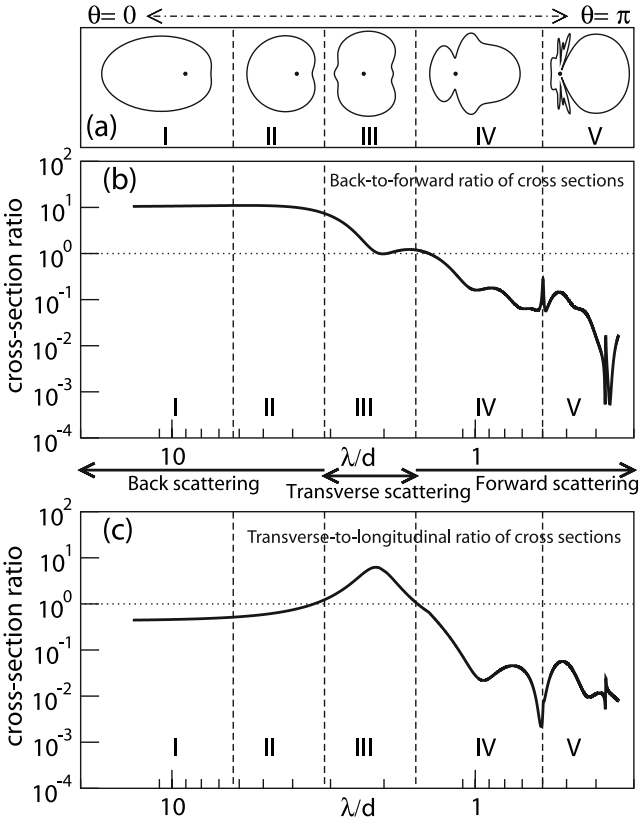

Figure 4. (a) Directivity patterns, i.e., the scattering of a plane wave coming from the right and incident on a spherical inclusion, computed for each frequency domain. (b) Back-to-forward ratio of scattering amplitude defined as $|f(0)|^2/|f(\pi)|^2$. Bands I and II and bands IV and V correspond to dominant back scattering and to dominant forward scattering, respectively. (c) Transverse-to-longitudinal ratio of scattering amplitude defined as $|f(\pi/2)|^2/\max\ [|f(\pi)|^2, |f(0)|^2]$. Band III corresponds to the frequency domain where transverse scattering is dominant. In all three plots, the vertical dashed lines indicate the experimental frequency limits defined from the wavelet response analysis.

in Figures 4b and 4c which represent the back-to-forward and transverse-to-longitudinal ratios of the scattered amplitudes, respectively.

[25] The curve of Figure 4b indicates that in the low-frequency bands I–II, the back-scattered energy is about 1 order of magnitude larger than the energy re-radiated in the forward direction. The energy ratio is constant and equal to 10 in domain I and begins to decrease in domain II. The low-frequency bands correspond to a dominant back-scattering regime. The energy balance in the high-frequency bands IV–V is opposite to what happens in bands I–II with the forward scattered energy about one, and even two, orders of magnitude larger than the energy reradiated in the backward direction. The high-frequency bands correspond to a dominant forward scattering regime where most of the incident energy is scattered deeper in the bead layer. The experimental limit between domains IV–V falls on a strong perturbation of both the back-to-forward and transverse-to-longitudinal ratios of cross sections corresponding to a sharp Mie resonance line.

[26] The curve of the transverse-to-longitudinal energy ratio (Figure 4c) possesses an absolute maximum centered in band III which separates the low-frequency domain where the layer of glass beads behaves as a simple reflector, i.e., the conical pattern of the wavelet response in Figure 3b, and the high-frequency range where the layer of beads behaves as a random medium re-radiating a diffuse wavefield. Band III is also remarkable in the sense that the backscattered and forward scattered energies are equal for $\lambda = 2d$ where the transverse-scattered energy is maximum, up to 1 order of magnitude larger than the longitudinal-scattered energy (Figure 4c). The intermediate frequency band then corresponds to a dominant transverse-scattering regime. Both experimental frequency limits of domain III correspond to the equilibrium between the transverse-to-longitudinal energy ratio, as predicted by the scattering patterns for a single scatterer.

[27] The frequency bands identified from the experimental data correspond to particular radiation diagrams computed for a single bead: the macroscopic response of the monodisperse granular medium appears to be controlled by scattering processes at the microscopic scale. Each scatterer contributes coherently in the mean reflected field inducing a strong link between the behavior of a single bead and that of many. In particular, note the semblance between the reflectivity curve (Figure 3b) representative of the energy reflected by the whole granular medium, and the back-to-forward energy ratio (Figure 4b) representative of the energy reflected by a single glass bead. We can interpret the strong decrease in the wavelet response amplitude, observed in band III of the ridge function curves (Figure 3b), as a significant amount of the incident wave energy reradiated perpendicularly to the incident direction. The similarity we found with results from single scattering model occurs in the mean-field measurements of the backscattered energy where multiple-scattering processes are averaged in the experimental results.

3.3. Propagation-to-Diffusion Transition

[28] We now consider in more details what happens in the wavelength band III which corresponds to the transition between the long-wavelength domain, where the granular medium is equivalent to a simple localized reflector, and the short-wavelength domain, where multiple scattering occurs and induces back-scattered coda wavefield. The wavelet response method allows for separating the ballistic wave and the coda waves to perform a quantitative study of the energy balance between these two components of the back-scattered wavefield. The time of the ballistic arrival (dotted curve in Figure 3a) corresponding to the reference wavelet response of Figure 1b is used to distinguish the coherent ballistic reflection from the late arrivals forming the coda. We calculate the associated energies E_b and E_c by integrating the two signal components, respectively. The ballistic-to-coda energy ratio E_b/E_c is plotted as a function of λ/d in a log-log diagram (Figure 5a).

[29] The ballistic energy is 1 order of magnitude larger than the coda energy in domains I–II and down to 2 orders of magnitude smaller in domains IV–V. At low frequencies, the reflected energy comes from coherent reflection at

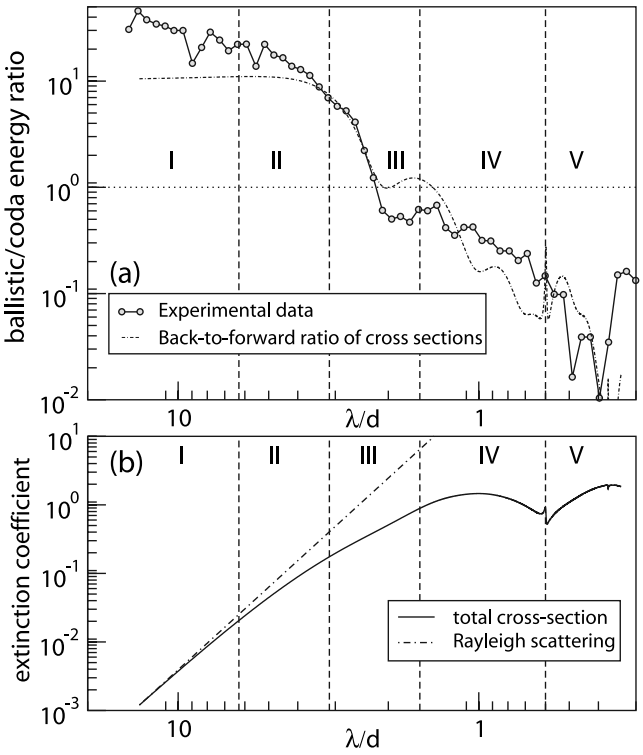

Figure 5. (a) Experimental curve representing the energy ratio between the ballistic energy and the back-scattered energy extracted from the wavelet response of the glass bead layer (see Figure 3a). Domain III corresponds to the transition between a propagation regime to a diffusion regime, identified in the domains I–II and IV–V, respectively. (b) Extinction coefficient (solid line), i.e., total scattering cross section divided by the geometrical cross section $\pi\, d^2/4$. Also shown are the five frequency bands identified in the data (see Figure 3). In band I, the scattering cross section closely follows the Rayleigh scattering power law ($\propto\lambda^{-4}$) (dashed line).

the interface, whereas it is mainly associated to multiple scattering at high frequencies where the scattered waves follow long tortuous paths in the heterogeneous medium.

[30] In frequency band I, the extinction coefficient follows a Rayleigh scattering law $\propto\lambda^{-4}$ [*Ishimaru*, 1978] (Figure 5b) indicating a single-scattering regime inside the granular medium when $\lambda > 2\pi d$ where propagation dominates. In domain II, transverse scattering increases for a single bead (Figure 4c), and the single-scattering regime is less and less valid. Domains IV–V correspond to multiple-scattering regime.

[31] At intermediate frequencies of domain III, the energies of the ballistic component and the coda are equivalent when $\lambda = 2d$, corresponding to a strong transition of a propagation regime at low frequencies to a diffusion regime at high frequencies. These experimental results on mean-field measurements (solid line in Figure 5a) are similar to the theoretical curve of the back-to-forward scattering energy ratio computed for a single glass bead (dotted line in Figure 5a) which microscopic coherency induces the macroscopic behavior of the granular medium.

4. Effective Medium Theories

4.1. Single-Scattering Regime

[32] We now consider effective medium models and consider their efficiency to reproduce the experimental reflectivity curve discussed in sections 2 and 3. A first class of models concerns the quasi-static models whose effective medium properties do not depend on the frequency. This is for instance the case of the models proposed by *Kuster and Toksöz* [1974] and by *Berryman* [1980] in the context of geophysical applications. These models are fully constrained by the experimental physical and geometrical properties of the granular medium, namely the shape, size, concentration and nature of both the inclusions (i.e., glass beads) and the fluid matrix (i.e., water). The models of *Kuster and Toksöz* [1974] and of *Berryman* [1980] are both derived by considering the statistical properties of a large number of elastic spherical inclusions randomly dispersed in a fluid matrix. The diffusing spheres of diameter d occupy a volume fraction ϕ and their scattered far field is computed for signal wavelengths $\lambda \gg d$ using the single-scattering approximation. The physical properties of the equivalent homogeneous medium are the effective density, ρ^*, and the effective compressibility modulus K^*.

[33] In the model of *Kuster and Toksöz* [1974], the cluster of spheres embedded in the fluid matrix is replaced by a homogeneous equivalent sphere such that the scattered far field is unchanged in the fluid matrix. With this constrain, the effective density ρ^*_{KT} of the effective medium is a real-valued quantity given by

$$\frac{\rho_{\mathrm{m}} - \rho^*_{KT}}{\rho_{\mathrm{m}} + 2\rho^*_{KT}} = \phi\,\frac{\rho_{\mathrm{m}} - \rho_{\mathrm{s}}}{\rho_{\mathrm{m}} + 2\rho_{\mathrm{s}}}, \tag{6}$$

where ρ_s and ρ_m are the densities of the spherical inclusions and the fluid matrix, respectively. The concentration of elastic inclusions in the fluid matrix is $0.74 > \phi \geq 0$. The effective compressibility modulus K^*_{KT} is defined by Wood's law:

$$\frac{1}{K^*} = \frac{\phi}{K_s} + \frac{1-\phi}{K_m}, \tag{7}$$

where K_s and K_m are the compressibility moduli of the spherical inclusions and the fluid matrix, respectively.

[34] In the model of *Berryman* [1980], the same cluster of spherical inclusions in material s embedded in a fluid matrix m is replaced by a compound of inclusions in a homogeneous equivalent matrix * such that no scattered field is radiated outside the cluster of inclusions in material i and m, respectively, embedded in the effective medium *. Under this constrain, the effective density ρ^*_B is a real-valued parameter defined by

$$\frac{1}{\rho^*_B + \frac{1}{2}\rho^*_B} = \frac{\phi}{\rho_{\mathrm{s}} + \frac{1}{2}\rho^*_B} + \frac{1-\phi}{\rho_{\mathrm{m}} + \frac{1}{2}\rho^*_B}. \tag{8}$$

Note that formula (8) for the effective density is symmetric under interchange of constituent labels, m for the fluid

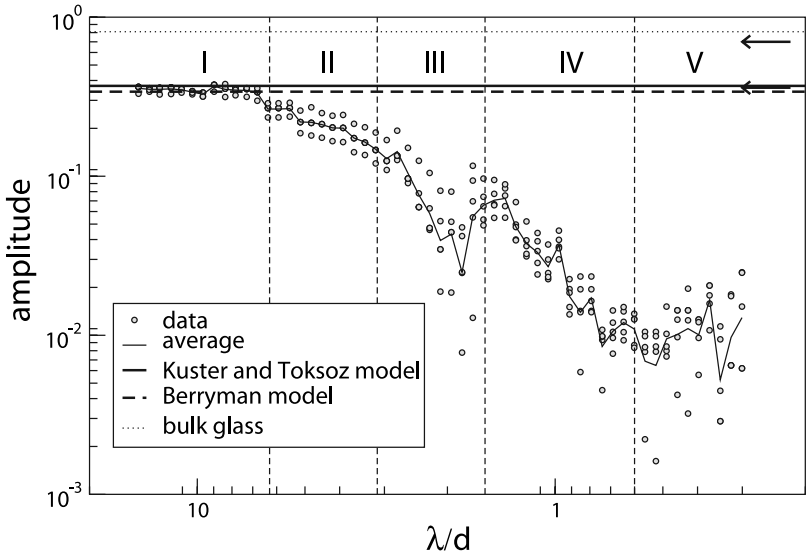

Figure 6. Experimental reflectivities (dots and solid line) extracted from the granular medium wavelet response superimposed with the equivalent theoretical reflectivities $\gamma^*_{KT} = 0.34$ and $\gamma^*_B = 0.37$ computed from *Kuster and Toksöz* [1974] and *Berryman* [1980], respectively (dashed vertical lines). The dashed horizontal line stands for the reflectivity $\gamma = 0.81$ of a pure bulk glass. The horizontal arrows in the upper right part of the graph represent the upper and lower reflectivity bounds of *Hashin and Shtrikman* [1963].

matrix and s for the spherical inclusions which concentrations are $(1 - \phi)$ and ϕ, respectively.

[35] The effective velocity c^* of the fluid equivalent homogeneous medium is a real value and the effective reflectivity γ^* follows the real acoustic impedance contrast expressed in equation (9):

$$c^* = \sqrt{K^*/\rho^*}, \qquad \gamma^* = \frac{\rho^* c^* - \rho_m c_m}{\rho^* c^* + \rho_m c_m}, \tag{9}$$

where $c_m = 1480$ m/s and $\rho_m = 1000$ kg/m^3 is the sound velocity and density of water, respectively.

4.2. Multiple-Scattering Regime

[36] *Waterman and Truell* [1961] have proposed an effective medium theory taking multiple scattering into account. This model has been applied to the problem of an elastic wave scattered by a finite number of inclusions inside a homogeneous matrix [*McClements and Povey*, 1989; *Anson and Chivers*, 1993; *Robert et al.*, 2004]. This model also considers the case of spherical scatterers embedded in a fluid matrix. The model is fully constrained by the physical parameters of the experimental granular medium. The properties of the effective equivalent medium are frequency-dependent, and the model of *Waterman and Truell* [1961] belongs to the so-called class of dynamic effective models.

[37] From a granular medium made of spherical inclusions, *Waterman and Truell* [1961] define an equivalent homogeneous medium whose effective properties are characterized by complex value parameters, the imaginary part of which stands for scattering absorption. The effective medium wave number k^*, expressed by

$$\left(\frac{k^*}{k_m}\right)^2 = \left(1 + \frac{2\pi n f(0)}{k_m^2}\right)^2 - \left(\frac{2\pi n f(\pi)}{k_m^2}\right)^2, \tag{10}$$

is complex valued owing to the scattering parameters $f(0)$ and $f(\pi)$ which are the diffusion amplitudes of a single scatterer in the back- and forward scattering direction, respectively (see *Sheng* [1995] for details). The wave number k_m is the (real) wave number in the fluid matrix and $n = 6\phi/\pi d^3$ is the number of elastic spherical inclusions per volume unit. The inclusions are supposed to be uniformly distributed.

[38] From equation (10), the effective velocity of the equivalent fluid medium is also a complex-valued quantity and is expressed in equation (11) corresponding to the effective medium immersed in water (c_m and k_m are the sound velocity and the wave number in the water, respectively). The effective reflectivity γ^* following the acoustic impedance contrast is given by equation (11) (the reflection coefficient of the glass bead layer is defined as the modulus of the effective reflectivity):

$$c^* = c_m \frac{k_m}{k^*}, \qquad \left|\gamma^*\right| = \left|\frac{\rho^* c^* - \rho_m c_m}{\rho^* c^* + \rho_m c_m}\right|. \tag{11}$$

5. Comparison With the Experimental Data and Discussions

5.1. Very Long Wavelength Domain

[39] Identified from the experimental wavelet response, domain I is characterized by five ridge functions which slope is $\alpha = 0$ in a log-log diagram for wavelengths $\lambda > 2\pi d$ (Figure 3b). In this frequency band, the interface between water and the layer of glass beads can be represented by a sharp Heaviside-like interface between water and an equivalent homogeneous medium with frequency-independent properties. The reflected field is measured in the far-field condition and the extinction coefficient curve plotted in

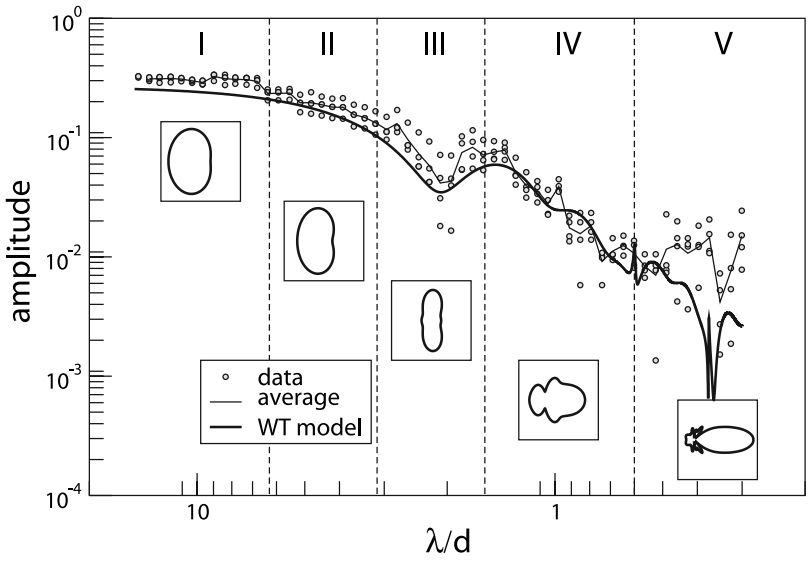

Figure 7. Experimental reflectivities superimposed with the predictions of the dynamic model of *Waterman and Truell* [1961]. Also shown are the five experiment frequency bands and the associated directivity patterns at the local scale of a glass bead.

Figure 5b shows the wave phenomenon at work in band I is a Rayleigh single-scattering regime.

[40] Using the physical properties of experimental granular medium, the characteristics of the effective medium given by the models of *Kuster and Toksöz* [1974] and of *Berryman* [1980] may be computed to obtain the effective reflectivity γ^*. We obtain $\gamma^*_{KT} = 0.34$ and $\gamma^*_B = 0.37$ for the models of *Kuster and Toksöz* [1974] and of *Berryman* [1980], respectively. As can be seen in Figure 6, these theoretical reflectivity coefficients are in good agreement with the experimental curve in domain I. Also shown for comparison is the reflectivity $\gamma = 0.81$ of bulk glass. Even if no confining pressure is applied on the close packing of spherical inclusions, percolating stress network should exist through the Hertz contacts among the glass beads [*Rioual et al.*, 2003]. This effect should contribute to the efficiency of the granular medium reflectivity but it does not appear in the methods of *Kuster and Toksöz* [1974] and *Berryman* [1980]: the effect is then supposed to be very weak in our experiments.

5.2. Intermediate-Wavelength Domain

[41] In the frequency bands II-III-IV, the experimental reflectivity curve (Figure 3b) displays a strong dependence of the reflectivity with the wavelength of the incident wave and the wave phenomena involved in each band are different. The Rayleigh scattering occurring in band I ceases to be valid in band II, and a dominant lateral scattering occurs in band III where by a strong decrease in the reflected energy is observed. Band IV is dominated by strong forward scattering which produces a long coda wave formed by the scattered waves coming from deeper parts of the heterogeneous medium (see Figure 3a). In these intermediate frequencies, we cannot apply quasi-static methods and we work on dynamic effective medium methods as the theory proposed by *Waterman and Truell* [1961].

[42] All physical parameters are controlled in our experiments and none has to be adjusted. We compute the model of *Waterman and Truell* [1961] for a large frequency range, i.e., between 100 kHz and 5 MHz, and for 63% of $d = 1$ mm glass beads immersed in water. The theoretical results are plotted in Figure 7 together with the experimental reflectivity curve. The theoretical reflectivity predicted by Waterman and Truell is in good agreement with the data over a large frequency range including the low-frequency domain I. It slightly underestimates the data in domains I, II, and III, where the reflectivity decrease measured around $\lambda = 2d$ is also well predicted by the theory. In domain IV, the effective medium theory of *Waterman and Truell* [1961] fits very well the experimental data. Also note the theoretical resonance located on the high-frequency limit $\lambda \simeq 2\ d/\pi$. In domain V, we observe a significant discrepancy between the model and the data, discussed in section 5.3.

[43] From equations (11), we compute the effective velocity c^* of the granular medium and plot the modulus in Figure 8 as a function of λ/d for frequencies ranging from 100 kHz and 5 MHz. We observe strong variations of the effective velocity between 1930 m/s and 1350 m/s for the low and intermediate frequencies, respectively. In domains

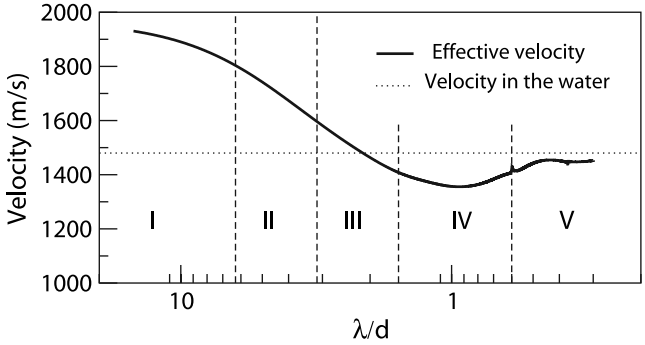

Figure 8. Modulus of the effective velocity for a granular medium made of glass beads calculated from the dynamic model of *Waterman and Truell* [1961].

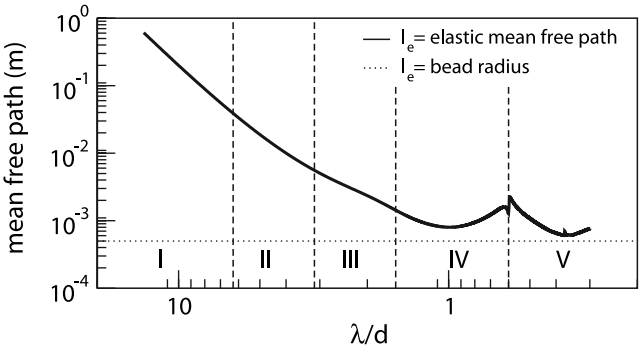

Figure 9. Elastic mean free path. In band V, it reaches the glass bead radius. This means that the wave does not penetrate inside the medium and that the first bead layer reflects the incident wave.

I–II and IV–V, the effective velocity $|c^*|$ is larger and smaller, respectively, than the sound velocity in the fluid matrix c_m = 1480 *m/s* and $|c^*| = c_m$ when $\lambda/d = 2$ in domain III. At low frequencies, the resulting effective velocity $|c^*| > 1600$ *m/s*: the acoustic waves propagate through the glass beads which sound velocity is much larger than c_m. In the high-frequency domain, the acoustic waves are multiple scattered inside the granular medium before being re-radiated: the effective velocity is complex and the imaginary part arises from tortuosity effects induced by the glass beads. The acoustic waves mainly propagate through the matrix and follow longer paths around the glass beads, resulting in a smaller effective velocity.

5.3. Very Short Wavelength Domain

[44] In the high-frequency band, the model of *Waterman and Truell* [1961] is not in good agreement with the data. The data scatter is large in domain V, but in the average, the measurements are one order of magnitude larger than the model predictions when $\lambda < \pi d/2$ which is the frequency limit between domains IV and V. This high-frequency limit appears as the validity limit of the theory of Waterman and Truell. In domain V, multiple-scattering attenuation is important. The acoustic waves are strongly scattered by the glass beads and cannot propagate very deep inside the medium. In order to propose a theoretical interpretation of this limit, we study the elastic mean free path [see *Sheng*, 1995]. This multiple-scattering parameter, defined by equation (5), quantifies the distance traveled by the coherent waves inside the medium and is plotted versus λ/d in Figure 9.

[45] In the low-frequency bands I-II-III, the elastic mean free path is much larger than the bead diameter d: the waves propagate over large distances and multiple scattering involves a large number of interactions between the acoustic waves and the glass beads. This agrees with the model of *Waterman and Truell* [1961] which requires averaging of statistical quantities. In the high frequencies V, the elastic mean free path may be smaller than the bead diameter. Hence scattering occurs in the very first layers of glass beads and no wave can propagate deep inside the granular medium: this makes volume averaging effects insignificant when $\lambda < 2d/\pi$ and the model of Waterman and Truell is not in accordance with the data in domain V.

[46] In the high-frequency band V, the experimental data tend to be frequency-independent with a ridge function characterized by a slope $\alpha \simeq 0$ (Figure 3b). The granular medium appears to be equivalent to a homogeneous medium defined by rough interface which induces scattering. The average reflectivity of this equivalent interface is $\gamma^* \simeq 0.01$ and takes surface scattering attenuation into account.

6. Conclusion

[47] From the wavelet response method, we define a coherent acoustic response over a large frequency range for a perfect reflector. We extend the analysis to characterize granular media with dense packing of glass beads saturated with water. We increase the frequency range by rescaling and merging the individual wavelet responses measured for different monodisperse layers of glass beads with different diameters, respectively. The global wavelet response spans a 5-octave frequency range, and the dimensionless parameter λ/d varies from 0.3 to 15 (Figure 3). We identify five ranges from the experimental wavelet response and define the frequency limits at $\lambda = 2d\pi$, $\lambda = d\pi$, $\lambda = \pi\, d/2$ and $\lambda = 2d/\pi$.

[48] In the low-frequency bands I and II, defined for $\lambda > 2d\pi$, we observe a coherent structure in the wavelet response where back scattering dominates. The ridge functions are linear curves with slopes $\alpha = 0$ and $\alpha = +1$ for domains I and domain II, respectively. In domain I, we show the existence of Rayleigh scattering where the granular medium can be replaced by an equivalent elastic and homogeneous medium defined by frequency-independent physical parameters. We apply quasi-static effective theories to define the effective properties and show good agreement between the experimental data and the theoretical predictions from *Kuster and Toksöz* [1974] and *Berryman* [1980].

[49] In domain II, where $2d\pi > \lambda > d\pi$, we observe a simple and coherent structure in the wavelet response but a frequency dependence of the ridge function amplitudes. We show that the Rayleigh scattering is not valid and that multiple scattering appears inside the granular medium. In order to describe the experimental data, we apply the dynamic effective medium theory developed by *Waterman and Truell* [1961] which takes multiple scattering into account. We put in evidence a very good agreement between the theoretical predictions and the data over both a large frequency range and a densely packed granular medium.

[50] We show that the intermediate domain III is characterized by strong transition phenomena: we observe a pronounced decrease of the back-scattered wavefield energy. We analyze the theoretical scattering for single glass bead and associate this observation to a dominant lateral scattering (Figure 4b). From the experiments, we define the limits of domain III by $\lambda = \pi d$ and $\lambda = \pi d/2$. In this domain, an equilibrium between the longitudinal and the transversal scattering dominates when $\lambda = 2d$ and we put in evidence a transition from the propagation regime to a multiple-scattering regime at low frequencies and high frequencies, respectively.

[51] In the higher-frequency domains IV and V, we show a dominant forward scattering for a single scatterer in accordance with multiple-scattering phenomena observed with the existence of coda wave in the wavelet response.

[52] From the wavelet response experiments we perform in highly concentrated granular media, we observe scattering phenomena and quantify the results from theoretical approach based on effective medium methods. We study in details the influence of the ratio λ/d on the granular medium reflectivity curve. This work, where we associate experimental and theoretical results, can help in the understanding of acoustic probing of geological interfaces.

[53] **Acknowledgments.** We thank Frédéric Conil for his help when constructing the wavelet family and Michel Lemoine, who helped us in designing the experimental setup. This work is financially supported by the CNRS and ANDRA through the GdR FORPRO (Research action 99.II) and corresponds to GdR FORPRO contribution 2006/10 A.

References

Acosta, J., M. Canals, A. Carbó, A. Muñoz, R. Urgeles, A. Muñoz-Martín, and E. Uchupi (2004), Sea floor morphology and Plio-Quaternary sedimentary cover of the Mallorca Channel, Balearic Islands, western Mediterranean, *Mar. Geol.*, *206*, 165–179.

Alexandrescu, M., D. Gibert, G. Hulot, J.-L. Le Mouël, and G. Saracco (1995), Detection of geomagnetic jerks using wavelet analysis, *J. Geophys. Res.*, *100*, 12,557–12,572.

Alexandrescu, M., D. Gibert, G. Hulot, J.-L. Le Mouël, and G. Saracco (1996), Worldwide wavelet analysis of geomagnetic jerks, *J. Geophys. Res.*, *101*, 21,975–21,994.

Anson, L. W., and R. C. Chivers (1993), Ultrasonic velocity in suspensions of solids in solids—A comparison of theory and experiment, *J. Phys. D*, *26*, 1566–1575.

Aristégui, C., and Y. C. Angel (2002), New results for isotropic point scatterers: Foldy revisited, *Wave Motion*, *36*, 383–399.

Augustin, J. M., R. Le Suave, X. Lurton, M. Voisset, S. Dugelay, and C. Satra (1996), Contribution of the multibeam acoustic imagery to the exploration of the sea-bottom, *Mar. Geophys. Res.*, *18*, 459–486.

Berryman, J. G. (1980), Long-wavelength propagation in composite elastic media: Spherical inclusions, *J. Acoust. Soc. Am.*, *68*, 1809–1819.

Berryman, J. G., and P. A. Berge (1996), Critique of two explicit schemes for estimating elastic properties of multiphase composite, *Mech. Mater.*, *22*, 149–164.

Burridge, R., G. Papanicolaou, and B. White (1988), One-dimensional wave propagation in a highly discontinuous medium, *Wave Motion*, *10*, 19–44.

Burridge, R., M. V. De Hoop, K. Hsu, L. Le, and A. Norris (1993), Waves in stratified viscoelastic media with microstructure, *J. Acoust. Soc. Am.*, *94*, 2884–2894.

Busch, K., and C. M. Soukoulis (1996), Transport properties of random media: An energy-density CPA approach, *Phys. Rev. B*, *54*, 893–899.

Carter, L. (1992), Acoustical characterization of seafloor sediments and its relationship to active sedimentary processes in Cook Strait, New Zealand, *N. Z. J. Geol. Geophys.*, *35*, 289–300.

Chambers, K., A. Deuss, and J. H. Woodhouse (2005), Reflectivity of the 410-km discontinuity from PP and SS precursors, *J. Geophys. Res.*, *110*, B02301, doi:10.1029/2004JB003345.

Chýlek, P., G. Videen, W. Geldart, S. Dobbie, and W. Tso (2000), Effective medium approximation for heterogeneous particles, in *Light Scattering by Non-spherical Particles: Theory, Measurements, and Geophysical Applications*, pp. 273–308, edited by M. Mishchenko, J. W. Hovenier, and L. D. Travis, Elsevier, New York.

Conil, F., D. Gibert, and F. Nicollin (2004), Nonlinear synthesis of input signals in ultrasonic experimental setups, *J. Acoust. Soc. Am.*, *115*, 246–252.

Cowan, M. L., K. Beaty, J. H. Page, Z. Liu, and P. Sheng (1998), Group velocity of acoustic waves in strongly scattering media: Dependence on the volume fraction of scatterers, *Phys. Rev. E*, *58*(5), 6626–6635.

De Moustier, C., and H. Matsumoto (1993), Seafloor acoustic remote sensing with multibeam echo-sounders and bathymetric sidescan sonar systems, *Mar. Geophys. Res.*, *15*, 27–42.

Derode, A., A. Tourin, and M. Fink (1998), Time reversal in multiply scattering media, *Ultrasonics*, *36*, 443–447.

Dineva, P. S., G. D. Manolis, and T. V. Rangelov (2006), Sub-surface crack in an inhomogeneous half-plane: Wave scattering phenomena by BEM, *Eng. Anal. Boundary Elements*, *30*(5), 350–362.

Exon, N. F., G. R. Dickens, J.-M. Auzende, Y. Lafoy, P. A. Symonds, and S. Van de Beuque (1998), Gas hydrates and free gas on the Lord Howe Rise, Tasman Sea, *PESA J.*, *26*, 148–158.

Foldy, L. L. (1945), The multiple scattering of waves: I. General theory of isotropic scattering by randomly distributed scatterers, *Phys. Rev.*, *67*, 107–119.

Goff, J. A., H. C. Olson, and C. S. Duncan (2000), Correlation of side-scan backscatter intensity with grain-size distribution of shelf sediments, New Jersey margin, *Geo Mar. Lett.*, *20*(3), 43–49.

Goodman, R. R., and R. Stern (1962), Reflection and transmission of sound by elastic spherical shells, *J. Acoust. Soc. Am.*, *34*(3), 338–344.

Gutowski, M., J. Bull, T. Henstock, J. Dix, P. Hogarth, T. Leighton, and P. White (2002), Chirp sub-bottom profiler source signature design and field testing, *Mar. Geophys. Res.*, *23*, 481–492.

Hashin, Z., and S. Shtrikman (1963), A variational approach to the theory of the elastic behavior of multiphase materials, *J. Mech. Phys. Solids*, *2*, 127–140.

Herrmann, F. J. (1994), Scaling of the pseudo primary analyzed by the wavelet transform, paper presented at the 64th meeting of SEG, Soc. of Explor. Geophys., Tulsa, Okla.

Herrmann, F. J., and J. J. Staal (1996), Waves in scaling media, the implication of non-differentiability, in *58th Annual EAGE Conference*, edited by D. J. Feenstra, Abstract C007, Eur. Assoc. of Geosci. and Eng, Amsterdam.

Holschneider, M. (1995), *Wavelets: An Analysis Tool*, 423 pp., Clarendon, Oxford, U. K.

Ishimaru, A. (1978), *Wave Propagation and Scattering in Random Media*, IEEE Press, Piscataway, N. J.

Kostylev, V. E., B. J. Todd, G. B. J. Fader, R. C. Courtney, G. D. M. Cameron, and R. A. Pickrill (2001), Benthic habitat mapping on the Scotian Shelf based on multibeam bathymetry, surficial geology and sea floor photographs, *Mar. Ecol. Prog. Ser.*, *219*, 121–137.

Kuster, G. T., and M. N. Toksöz (1974), Velocity and attenuation of seismic waves in two-phase media: Theoretical formulation, *Geophysics*, *39*, 587–618.

Lambert, D. N., M. T. Kalcic, and R. W. Faas (2002), Variability in the acoustic response of shallow-water marine sediments determined by normal-incident 30-kHz and 50-kHz sound, *Mar. Geol.*, *182*, 179–208.

Le Gonidec, Y., D. Gibert, and J. Proust (2002), Multiscale analysis of waves reflected by complex interfaces: Basic principles and experiments, *J. Geophys. Res.*, *107*(B9), 2184, doi:10.1029/2001JB000558.

Le Gonidec, Y., F. Conil, and D. Gibert (2003), The wavelet response as a multiscale NDT method, *Ultrasonics*, *41*, 487–497.

Le Gonidec, Y., G. Lamarche, and I. C. Wright (2005), Inhomogeneous substrate analysis using EM300 backscatter imagery, *Mar. Geophys. Res.*, *24*, 305–321.

Mallat, S., and W. L. Hwang (1992), Singularity detection and processing with wavelets, *IEEE Trans. Inf. Theory*, *38*, 617–643.

Marchetti, E., M. Ichihara, and M. Ripepe (2004), Propagation of acoustic waves in a viscoelastic two-phase system: Influence of gas bubble concentrationSingularity detection and processing with wavelets, *J. Volcanol. Geotherm. Res.*, *137*, 93–108.

Marsan, D., and C. J. Bean (1999), Multiscaling nature of sonic velocities and lithology in the upper crystalline crust: Evidence from the KTB Main Borehole, *Geophys. Res. Lett.*, *26*, 275–278.

McClatchie, S., R. E. Thorne, P. Grimes, and S. Hanchet (2000), Ground truth and target identification for fisheries acoustics, *Fish. Res.*, *47*, 173–191.

McClements, D. J., and M. J. W. Povey (1989), Scattering of ultrasound by emulsions, *J. Phys. D*, *22*, 38–47.

Neser, S., C. Bechinger, P. Leiderer, and T. Palberg (1997), Finite-size effects on the closest packing of hard spheres, *Phys. Rev. Lett.*, *7912*, 2348–2351.

O'Doherty, R. F., and N. A. Anstey (1971), Reflections on amplitudes, *Geophys. Prospect.*, *19*(3), 430–458.

Orange, D. L., J. Yun, N. Maher, and J. Barry (2002), Tracking California seafloor seeps with bathymetry, backscatter and ROVs, *Cont. Shelf Res.*, *22*, 2273–2290.

Page, J. H., H. P. Schriemer, A. E. Bailey, and D. A. Weitz (1995), Experimental test of the diffusion approximation for multiply scattered sound, *Phys. Rev. E*, *523*, 3106–3114.

Page, J. H., P. Sheng, H. P. Schriemer, I. Jones, X. Jing, and D. A. Weitz (1996), Group velocity in strongly scattering media, *Science*, *271*, 634–637.

Pecher, I. A., W. S. Holbrook, M. K. Sen, D. Lizarralde, W. T. Wood, D. R. Hutchinson, W. P. Dillon, H. Hoskins, and R. A. Stephen (2003), Seismic anisotropy in gas-hydrate- and gas-bearing sediments on the Blake Ridge, from a walkaway vertical seismic profile, *Geophys. Res. Lett.*, *30*(14), 1733, doi:10.1029/2003GL017477.

Price, P. B. (2006), Attenuation of acoustic waves in glacial ice and salt domes, *J. Geophys. Res.*, *111*, B02201, doi:10.1029/2005JB003903.

Rioual, F., A. Valance, and D. Bideau (2003), Collision process of a bead on a two-dimensional bead packing importance of the inter-granular contacts, *Europhys. Lett.*, *61*(2), 194–200.

Robert, S., J.-M. Conoir, H. Franklin, and F. Luppé (2004), Resonant elastic scattering by a finite number of cylindrical cavities in an elastic matrix, *Wave Motion*, *40*, 225–339.

Scales, J. A. (1993), On the use of localization theory to characterize elastic wave propagation in randomly stratified 1-D media, *Geophysics*, *58*, 177–179.

Schock, S. G., L. R. LeBlanc, and L. A. Mayer (1989), Chirp subbottom profiler for quantitative sediment analysis, *Geophysics*, *54*, 445–450.

Sheng, P. (1995), *Introduction to Wave Scattering, Localization and Mesoscopic Phenomena*, Elsevier, New York.

Sheng, P., Z. Q. Zhang, B. White, and G. Papanicolaou (1986), Multiple-scattering noise in one dimension: Universality through localization-length scaling, *Phys. Rev. Lett.*, *57*, 1000–1003.

Stevenson, I. R., C. McCann, and P. B. Runciman (2002), An attenuation-based sediment classification technique using Chirp sub-bottom profiler data and laboratory acoustic analysis, *Mar. Geophys. Res.*, *23*, 277–298.

Tournat, V., V. Pagneux, D. Lafarge, and L. Jaouen (2004), Multiple scattering of acoustic waves and porous absorbing media, *Phys. Rev. E.*, *70*, 026609, doi:10.1103/PhysRevE.70.026609.

Vandenplas, S., A. B. Temsamani, Z. Cisneros, and L. Van Biesen (2000), A frequency domain inversion method applied to propagation models in unconsolidated granular materials, *Ultrasonics*, *38*, 195–199.

Vanneste, M., M. De Batist, A. Golmshtok, A. Kremlev, and W. Versteeg (2001), Multi-frequency seismic study of gas hydrate-bearing sediments in Lake Baikal, Siberia, *Mar. Geol.*, *172*, 1–21.

Walter, D. J., D. N. Lambert, and D. C. Young (2002), Sediment facies determination using acoustic techniques in a shallow-water carbonate environment, Dry Tortugas, Florida, *Mar. Geol.*, *182*, 161–177.

Wapenaar, K. (1998), Seismic reflection and transmission coefficients of a self-similar interface, *Geophys. J. Int.*, *135*, 585–594.

Wapenaar, K. (1999), Amplitude-variation-with-angle behavior of self-similar interface, *Geophysics*, *64*, 1928–1938.

Waterman, P. C., and R. Truell (1961), Multiple scattering of waves, *J. Math. Phys.*, *2*, 512–537.

Wysession, M. E., E. A. Okal, and C. R. Bina (1992), The structure of the core-mantle boundary from diffracted waves, *J. Geophys. Res.*, *97*, 8749–8764.

D. Gibert, Géosciences Rennes, Université Rennes 1, B15 Campus de Beaulieu, F-35042 Rennes cedex, France. (gibert@univ-rennes1.fr)

Y. Le Gonidec, Géosciences Azur, B.P. 48 Port de la Darse, F-06235 Villefranche-sur-Mer, France. (legonidec@geoazur.obs-vlfr.fr)